Computers and Concrete, *Vol. 14, No. 6 (2014) 695-710*
DOI: http://dx.doi.org/10.12989/cac.2014.14.6.695

A nonlinear model for ultimate analysis and design of reinforced concrete structures

Konstantinos Morfidis[*1], Panos D. Kiousis[2a] and Hariton Xenidis[3b]

[1] *Institute of Engineering Seismology and Earthquake Engineering (EPPO-ITSAK), 55535, Pylaia, Thessaloniki, Greece*
[2] *Colorado School of Mines, Department of Civil and Environmental Engineering, Golden CO 80401*
[3] *Department of Civil Engineering, Aristotle University of Thessaloniki, Aristotle University campus, 54124, Thessaloniki, Greece*

(*Received March 15, 2014, Revised June 10, 2014, Accepted July 25, 2014*)

Abstract. This paper presents a theoretical and computational approach to solve inelastic structures subjected to overloads. Current practice in structural design is based on elastic analysis followed by limit strength design. Whereas this approach typically results in safe strength design, it does not always guarantee satisfactory performance at the service level because the internal stiffness distribution of the structure changes from the service to the ultimate strength state. A significant variation of relative stiffnesses between the two states may result in unwanted cracking at the service level with expensive repairs, while, under certain circumstances, early failure may occur due to unexpected internal moment reversals. To address these concerns, a new inelastic model is presented here that is based on the nonlinear material response and the interaction relation between axial forces and bending moments of a beam-column element. The model is simple, reasonably accurate, and computationally efficient. It is easy to implement in standard structural analysis codes, and avoids the complexities of expensive alternative analyses based on 2D and 3D finite-element computations using solid elements.

Keywords: reinforced concrete; elastoplastic; softening; nonlinear analysis; finite element method; interaction diagrams

1. Introduction

Accurate analysis and design of nonlinear structures subjected to overloads is an important issue in structural engineering. Common practice is based on elastic evaluation of the internal forces followed by limit design which is based on inelastic material behavior. This is implicitly equivalent to placing a sufficient number of plastic hinges at critical points, which are defined by elastic analysis, to produce structural collapse. Thus, an analysis that distributes internal forces based on the elastic relative stiffness of the structural members of the structure is followed by a design which is based on relative element strengths. Such an approach has served the structural

∗Corresponding author, Ph.D., Assistant Researcher, E-mail: konmorf@gmail.com
[a] Ph.D., Associate Professor, E-mail: pkiousis@mines.edu
[b] Ph.D., Associate Professor, E-mail: xharis@civil.auth.gr

 ISSN: 1598-8198 (Print), 1598-818X (Online)

designers reasonably well through the years. The main advantages come from the simplicity of the method, which satisfies equilibrium. A ductile structure redistributes its internal forces, and tends to fail in the way that it has been designed. The main disadvantages of this approach include suboptimal performance, potential unwanted inelastic behavior under service loads, and early cracking, especially in structures that are dominated by dead loads. The difficulty arises due to the fact that relative element stiffnesses within a structure change continuously under inelastic loading. This may lead to internal force tendencies that are different from the ultimate state that is enforced by the ultimate strength design and the associated plastic hinges. A potential and undesirable result of this approach is premature inelastic response, and cracking. Furthermore, under certain circumstances, the outcome may be unrealized strength under overloads due to unexpected internal force developments and moment reversals. It is thus suggested that inelastic analysis of structures is desirable. This need has been recognized in the past, and has been studied on the basis of advances approaches. Nonlinear structural analysis based on solid block finite elements has been presented in various studies (e.g. Stevens *et al*. (1991), Song *et al*. (2002), Hu *et al*. (2004), Gregori *et al*. (2007)). This approach can be computationally expensive, it requires a high level of modeling expertise, and may be hindered by computational instabilities when simulating softening element response. A second approach uses nonlinear springs at strategic locations within elastic elements (e.g. Powell and Chen (1986), Liew (1992), White (1993), Nanakorn (2004)). Such approaches enjoy significant computational advantages over the solid-blocks finite element method. However they do not associate the bending behavior (strength and ductility) with the axial loading of the element, thus limiting their accuracy. Distributed plasticity models, although less common, have also been presented in the past (e.g. Yüksel and Karadoğan (2009)). However, they also fail to associate the bending behavior with that of the axial loading of the element. Additional approaches have been presented where the classical elastoplastic constitutive equations are extended from the infinitesimal level to the structural element level for steel structures (e.g. King *et al*. (1992)) as well as for concrete structures (e.g. El-Metwally *et al*. (1990), Spacone *et al*. (1996), Karabinis and Kiousis (2001), Bouchaboub and Samai (2013)). These approaches introduce significant computational expediency compared to solid-blocks finite element approaches, and have improved accuracy compared to the nonlinear springs methods. However, they are all based on tangential (incremental) approaches, and as a result, they are not free of computational difficulties under softening load-deformation behavior, and may be difficult for practical use.

This paper presents a secant elastoplastic approach to simulate the response of concrete structural elements. This method is based on column-beam elements with stiffness matrix relations, which are based on nonlinear moment-curvature and axial force-deformation relations. These relations are combined with axial force – bending moment interaction diagrams, to properly evaluate the capacity of an element when subjected to combined loads. The goal of this approach is to develop a nonlinear mathematical formulation based on secant stiffness matrices, which are positive definite, even when softening behavior is encountered. The resulting equations can be incorporated to existing structural analysis software to produce an interactive analysis-design approach to structural design. It will be demonstrated that the present model can capture efficiently and quite accurately the inelastic response of structures subjected to overloads.

2. Method basics

2.1 The constitutive model principles

The constitutive equations of this model are based on the following principles:

a. The bending moment capacity M_n and axial force capacity N_n are based on a M_n – N_n interaction diagram.

b. The axial force-axial deformation relation is based on the instantaneous axial force capacity N_n.

c. The bending moment – curvature relation is based on the instantaneous bending moment capacity M_n.

2.2 Axial force response

Following Fig. 1, the uniaxial stress-strain diagram of concrete is modeled by the modified Hognestad (1955) pre-peak expression (Kent and Park (1971)):

$$f_c = -f'_{cc} \cdot \left[sign(\varepsilon) \cdot (\varepsilon / \varepsilon_{cc0})^2 + 2 \cdot (\varepsilon / \varepsilon_{cc0}) \right] \tag{1}$$

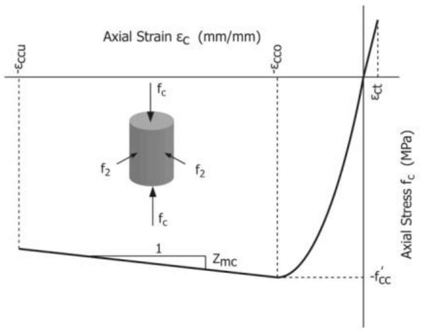

Fig. 1 Uniaxial stress-strain relation of confined concrete

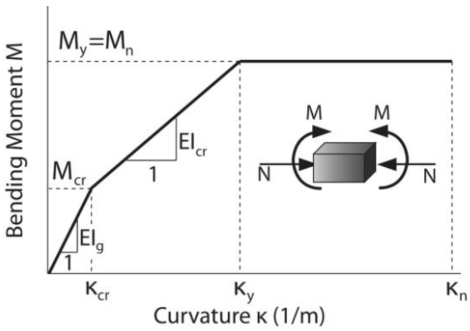

Fig. 2 Moment-curvature relation of a concrete element

where ε is the concrete strain (positive in tension), ε_{cc0} is the strain at the peak stress, f_c is the concrete stress (positive in tension), and f'_{cc} is compressive strength of concrete, based on its confinement.

The post-peak response of concrete up to the confined crushing strain ε_{ccu} is modeled as:

$$f_c = -f'_{cc} \cdot \left[1 + Z_{mc} \cdot \left(\varepsilon + \varepsilon_{cc0}\right)\right] \tag{2}$$

where Z_{mc} is a softening coefficient, which is a function of the amount of confinement. In the case of zero confinement, Z_{mc} and ε_{ccu} acquire their unconfined values Z_m, and ε_{cu} respectively, which are typically obtained from a compression cylinder test. It is noted that Z_{mc} is positive when expressing softening.

The post peak behavior of concrete in compression has been modeled in the past (Sharma (1990), Fantilli *et al*. (2007), Koshikawa (2013)). Sharma's approach (Sharma (1990)) is compatible to Eq. (2), and evaluates Z_{mc}, when stresses are expressed in MPa, as follows:

$$Z_{mc} = \frac{0.0034}{\dfrac{0.021 + 0.002 f'_c}{f'_c - 6.895} + \dfrac{3}{4} \cdot \rho_s \cdot \sqrt{\dfrac{b_c}{s}} - 0.002} \tag{3}$$

where ρ_s is the volumetric content of transverse reinforcement based on the confined core volume, b_c is the core width, and s is the transverse reinforcement spacing.

2.3 The moment curvature response

The moment-curvature relation of a concrete element is modeled in this study as described in Fig. 2. This relation is defined by three limit states in moment (M_{cr}, M_y and M_n) and three limit states in curvature (κ_{cr}, κ_y and κ_n) representing the first tensile rupture or crack, the yield state, and the ultimate fracture or failure. For the purposes of this analysis, the yield and failure moments are assumed to be equal (M_y=M_n). This results in the tri-linear relation presented in Fig. 2. Such behavior is a reasonable approximation for concrete elements with tensile reinforcement in one layer (CEB (1993)). The use of the tri-linear moment curvature relation of Fig. 2 is not necessary for the development of this model. However, it is adapted here for its simplicity. Thus, for a bending moment less than M_{cr}, the flexural rigidity is equal to E_cI_g where E_c=modulus of elasticity of concrete, and I_g= gross (or uncracked) moment of inertia. For moments M such that $M_{cr}<M<M_y$, the incremental flexural rigidity is equal to E_cI_{cr}, where I_{cr}=cracked moment of inertia.

The crack moment M_{cr}, as well as the yield moment M_y and failure moment M_n, are functions of the cross-sectional properties and are evaluated based on three distinct bending moment – axial force interaction diagrams which are described in the following sections.

2.4 Determining the rupture or crack state

Whereas tensile cracking occurs under elastic conditions in pure bending, this is not necessarily the case under combined compression and bending. The state of imminent tensile rupture is the locus of N and M combinations that are associated with the strain and stress state described

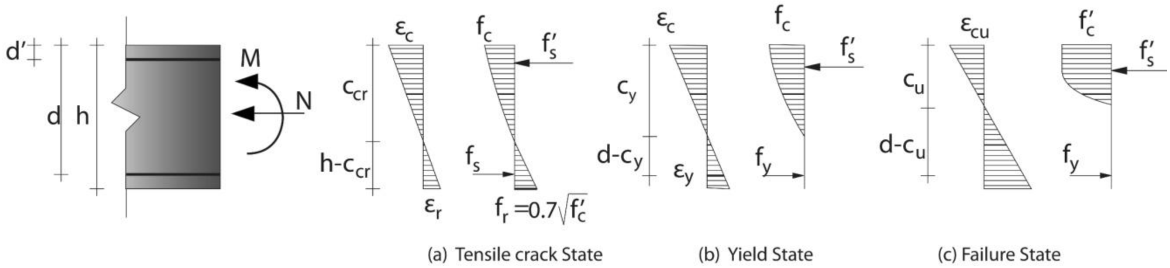

Fig. 3 Definition of states of (a) Tensile crack, (b) Yield and (c) Failure

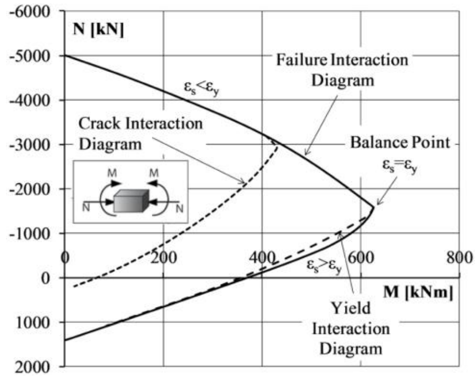

Fig. 4 Interaction Diagrams for the crack, yield, and failure states

in Fig. 3a. This is a state where the most tensile concrete strain corresponds to the rupture strain of concrete ε_r. Variations of the most compressive strain ε_c result in different combinations of N and M that produce the rupture or crack interaction diagram demonstrated in Fig. 4. For each point the curvature at the tensile crack state is defined as:

$$\kappa_{cr} = \varepsilon_r / \left(h - c_{cr}\right) \tag{4}$$

Thus, for any axial load N, the tensile crack moment M_{cr} and the corresponding curvature κ_{cr} are defined.

It is interesting to note that for axial compression that is larger than a specific magnitude (which depends on the column geometry and material properties), the tensile crack interaction diagram coincides with the failure interaction diagram indicating that above a specific axial compression, a cross-section fails before it ruptures in tension (Fig. 4).

2.4.1 Determining the yield state

The yield state is defined as the state where the tensile steel yields ($\varepsilon_s=\varepsilon_{sy}=f_y/E_s$=500MPa/200GPa=0.0025). This state is defined in Fig. 3b as the state where the tensile steel attains the yield strain ε_y. Variations of the most compressive strain ε_c result in different combinations of N and M that produce the yield interaction diagram demonstrated in Fig. 4. This state is meaningful only for M, N combinations that are below the balanced point. Load combinations above the balanced point result in brittle failures, where the tensile steel is, and yielding is not distinguished from failure. The curvature at yield is defined based on Fig. 3b as:

$$\kappa_y = \varepsilon_y \big/ \left(d - c_y \right) \tag{5}$$

Thus, for any axial load N, the bending moment at yield M_y and the corresponding curvature κ_y can be calculated. Based on the interactive relations at initial rupture, yield, and failure, the parameters of the moment curvature relation (Fig. 2) can be developed.

2.4.2 Determining the ultimate strength state

The ultimate strength state is defined as the state where concrete crushes in compression (Fig. 3c), where ε_c=ε_{cu}=0.0035. The process of developing the interaction diagram for failure is similar to the processes to develop the tensile crack and yield interaction diagrams. In this case, the most-compressive strain of concrete is set to ε_{cu}, and the tensile steel strain varies. Interactive relations of the axial force N_n, the bending moment M_n (Fig. 4) and the curvature κ_n at failure, are produced based on Fig. 3c and Eqs. (6), (7) and (8):

$$M_n = \int_0^{c_u} \left[-f_c(x) \cdot b \cdot \left(h/2 - c_u + x \right) \right] dx - A_s' \cdot f_s' \cdot \left(h/2 - d' \right) + A_s \cdot f_s \cdot \left(d - h/2 \right) \tag{6}$$

$$N_n = \int_0^{c_u} \left[f_c(x) \cdot b \right] dx + A_s' \cdot f_s' + A_s \cdot f_s \tag{7}$$

$$\kappa_n = \varepsilon_{cu} \big/ c_u \tag{8}$$

where b is the width of cross-section, h is the depth of the cross-section, d is the effective depth of the cross-section, A_s is cross-sectional area of the tensile reinforcement, A_s' is the cross-sectional area of the compression reinforcement, x is the distance of any point from the cross-sectional centroid, and c_u is the location of the neutral axis with respect to the most compressive fiber. Note that M_n, N_n and κ_n at failure are functions of the position of the neutral axis c_u.

2.4.3 Secant Load-deformation and Moment-curvature relations

The load-deformation relation (Eq. 2) describes the softening behavior that is typically observed in concrete under compression without sufficient confinement. The moment-curvature

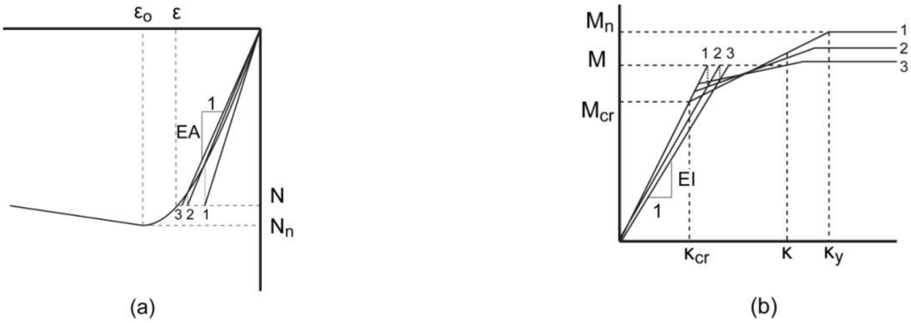

Fig. 5 Secant Load-Deformation Approach

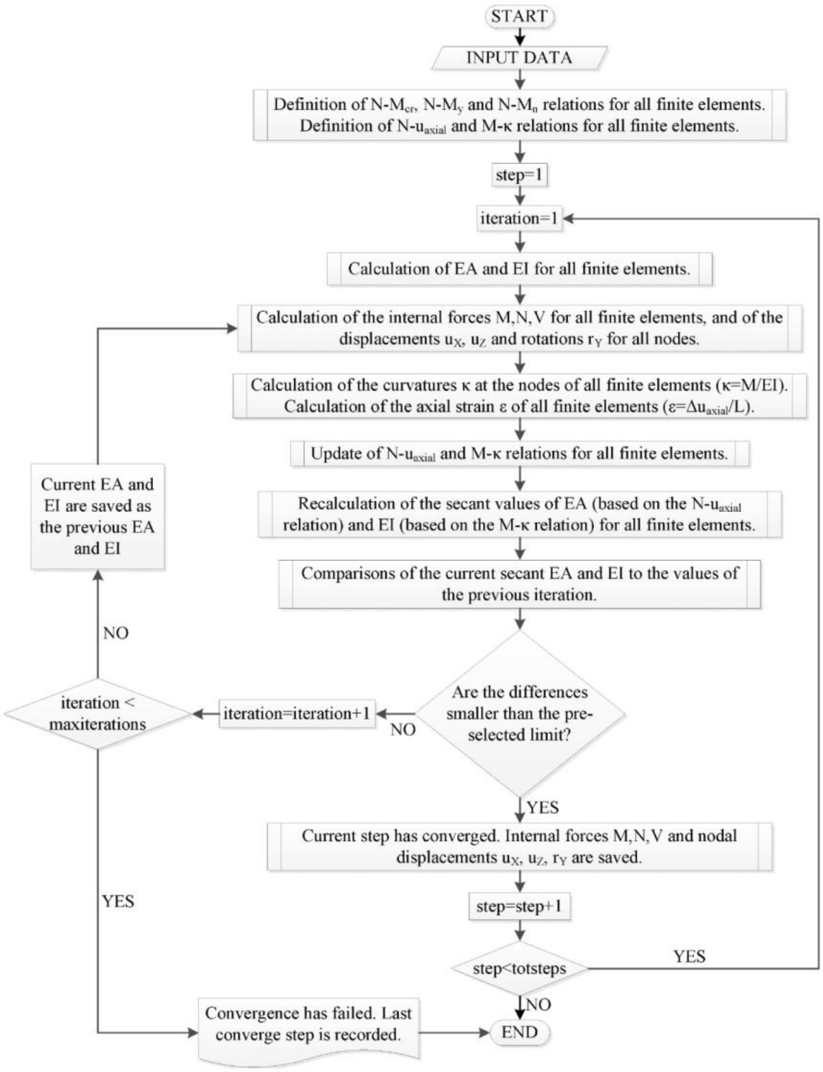

Fig. 6 Flowchart of the method

model (Fig. 2) does not exhibit softening under constant axial load. However, indirect bending softening can be developed under variable axial compression when this leads to a lower moment capacity (i.e. increasing N above balance, or decreasing N below balance).

Finite Elements modeling of softening material behavior using incremental load-deformation relations can result in computational difficulties due to the associated negative stiffness. Elastoplastic constitutive models are typically incremental in formulation and, when implemented in finite elements analysis, they must address the computational difficulties associated with negative stiffness.

In this analysis, a secant approach is implemented where the force-deformation and moment-curvature relations are expressed in terms of total quantities. The response of beam and column elements is modeled by defining instantaneous secant values of EA and EI as demonstrated in Fig. 5. These values are then applied into the standard stiffness matrix:

$$K = \begin{bmatrix} EA/L & 0 & 0 & -EA/L & 0 & 0 \\ 0 & 12EI/L^3 & 6EI/L^2 & 0 & -12EI/L^3 & 6EI/L^2 \\ 0 & 6EI/L^2 & 4EI/L & 0 & -6EI/L^2 & 2EI/L \\ -EA/L & 0 & 0 & EA/L & 0 & 0 \\ 0 & -12EI/L^3 & -6EI/L^2 & 0 & 12EI/L^3 & -6EI/L^2 \\ 0 & 6EI/L^2 & 2EI/L & 0 & -6EI/L^2 & 4EI/L \end{bmatrix} \tag{9}$$

The process is summarized as follows:

1. A structure is defined by its elements. For example, a structure may consist of six columns and 4 girders.
2. Additional discretization is applied based on anticipated inelastic response. For example, each girder may be divided in 20 elements, and each column may be divided in 10 elements.
3. For each element three interaction diagrams for tensile crack, yield and ultimate strength are defined (e.g. Fig. 4).
4. For each element, the relations of axial force vs displacement (Fig. 1), and bending moment vs curvature (Fig. 2) are defined.
5. It is noted that the moment-curvature relation continuously changes based on the instantaneous magnitude of axial force of the element based on the interaction diagrams of Fig. 4.
6. A load combination (N, V, M) is applied for every element.
7. The element matrices are formed using the current magnitudes of EA_1 and EI_1 (Fig. 5). The global stiffness matrix is formed and the problem is solved. New deformations and magnitudes of internal forces are calculated.
8. New secant values of EA_2 and EI_2 are calculated based on the new deformations. Note that the change in axial compression N (Fig. 5a) results in a change in the moment capacity of the cross-section (Fig. 5b). It is also noted that the axial force capacity also changes based on the developed moment as this is imposed by the axial force-bending moment interaction diagram (Fig. 4).
9. The element matrices are formed using EA_2 and EI_2. The global stiffness matrix is formed and the problem is solved again. New deformations and magnitudes of internal forces are calculated.
10. Steps 8 and 9 are repeated until convergence of the secant values of EA and EI is achieved.
11. The load combination (N, V, M) is increased to higher values (based on desired resolution of load deformation relations), and the process is repeated until the final load is applied.

The flowchart of this process is presented in Figure 6. It is noted that by following the above approach, the strength and stiffness of each element is automatically adjusted resulting in continuous internal force redistributions, up to the point that additional external forces cannot be satisfied internally, a) because they demand element strengths that cannot be provided, or b) because a sufficient number of plastic hinges is developed that result in static instability. At that point equilibrium cannot be satisfied and the global solution convergence is not possible.

3. Demonstration

The algorithm described above was implemented in a FORTRAN 2000 code to solve any two-dimensional frame structure with nonlinear behavior. The code was used to solve multiple examples, aiming to validate and calibrate the model. The examples that are presented here aim to: 1) demonstrate the basic concepts; 2) validate the results of the nonlinear analysis; and 3) demonstrate potential implications of nonlinear element response.

3.1 Example 1: Model validation - Comparison to tested frame

Cranston (1965) tested the frame presented in Fig. 7. This frame is used to validate the predictive capacity of the method. All elements of the frame have the same cross-section with reinforcement that includes 4#10 (metric) bars in tension and 2#10 bars in compression. The effective depth is d=138mm, while the compressive reinforcement depth is d'=14mm.

The nominal compression strength of concrete is f_c' =36.5MPa and the yield strength of the reinforcing steel is 293MPa. The experimental and predicted responses of the frame (load vs.

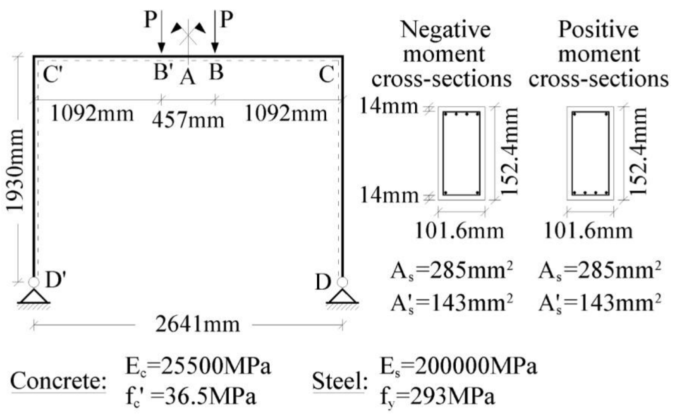

Fig. 7 Portal frame tested by Cranston (1965), Geometry and material data

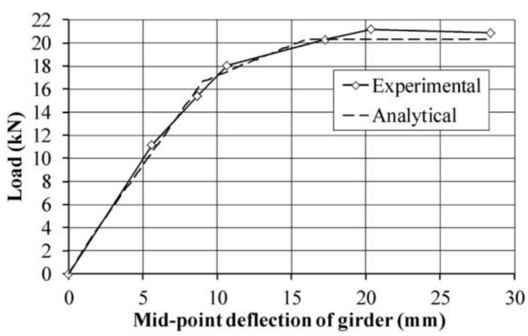

Fig. 8 Portal frame tested by Cranston (1965): Load vs mid-point deflection curves

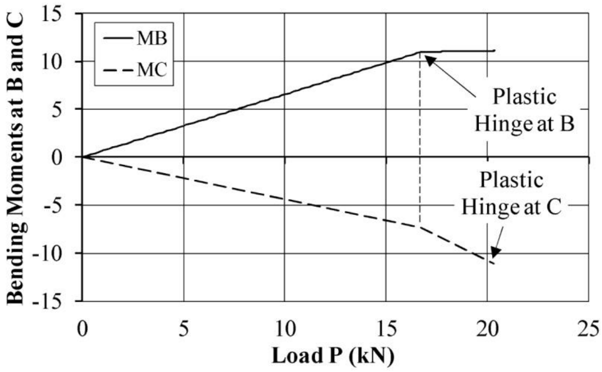

Fig. 9 Portal frame tested by Cranston (1965): Critical bending moment development

deformation) are presented in Fig. 8. Further analysis of Cranston's experiment is presented in Fig. 9, where the development of the bending moments at points B and C are presented as a function of the applied load. Note that a plastic hinge develops first at point B at load P=16.7kN and mid-point deflection 9.0mm followed by a second plastic hinge at point C, at load P=20.3kN and mid-point deflection 15.9mm. The formation of the first plastic hinge at B changes the structural system.

Added loads past the formation of plastic hinge at B are carried by section BC in a cantilever mode, which results in a super-linear increase of the moment at C. The formation of the second plastic hinge at point C results in structural instability (displacement controlled flow under constant load P).

3.2 Example 2: Extensive redistribution – Moment reversal

The second example presented here is a two-bay, one-story frame, demonstrated in Fig. 10. The frame is designed based on Eurocode 2 (2004) and Eurocode 8 (2004), such that the girders are reinforced with the maximum allowed steel content, while the columns are reinforced using the minimum allowed reinforcement. As will be demonstrated, this frame experiences extensive redistribution of internal forces that eventually lead to a reversal of the bending moment sign. The solutions presented here also examine the influence of axial compression softening (Z_{mc}), a behavior that is influenced by the column shape and amount of transverse reinforcement. The interaction diagrams for the elements of this structure are presented in Fig. 11.

The frame is loaded by a uniformly distributed load q_u to failure. The load-deformation of the central column, which is loaded by purely axial load, is presented in Fig. 12a. As expected, the column exhibits perfect plasticity when Z_{mc}=0, and it softens when Z_{mc}>0.

The inelastic axial compression of the mid-column results in moment reduction of the girder at point E (Fig. 12b). This reduction becomes more intense as Z_{mc} increases. It is seen that the frame is subjected to extensive redistribution of the internal moments (Fig. 12c) including sign reversal of the moment M_{ED}, which is accompanied by super-linear increase of all other support and corner bending moments. It is noted that the structural system changes once the middle column yields in axial compression. Any added load past this point is carried without the contribution of column BE and thus results in positive moment development at point E. This development is at accelerated rate (proportional to L^2, where L=10 m), and it results in an eventual complete reversal of the bending moment of the girder at point E. This example demonstrates that there exist circumstances that result in moment reversals that cannot be captured by the typical practice approach of elastic analysis followed by ultimate strength design.

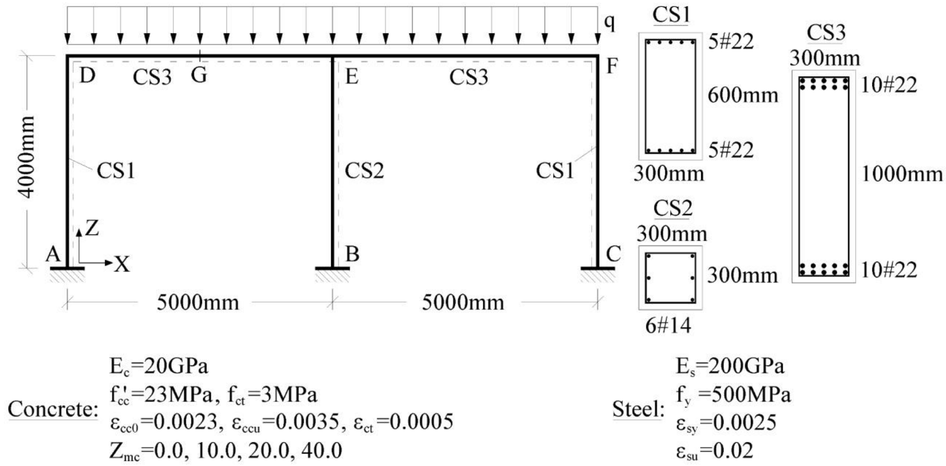

Fig. 10 Example of Two-bay, One-Story Frame

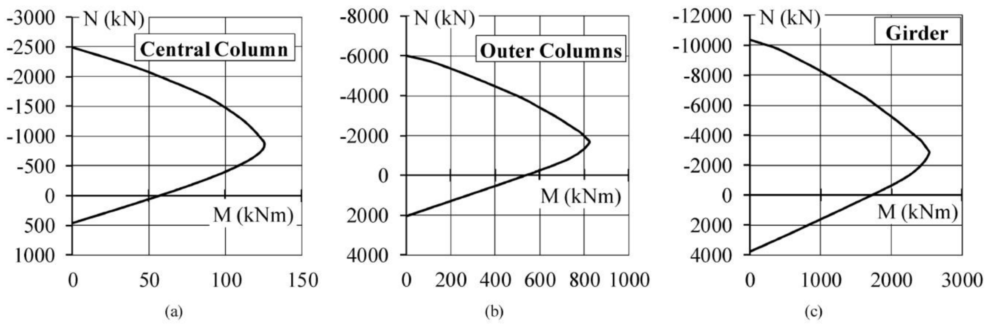

Fig. 11 Axial Force-Bending Moment Interaction Diagrams of the Elements of Example 2

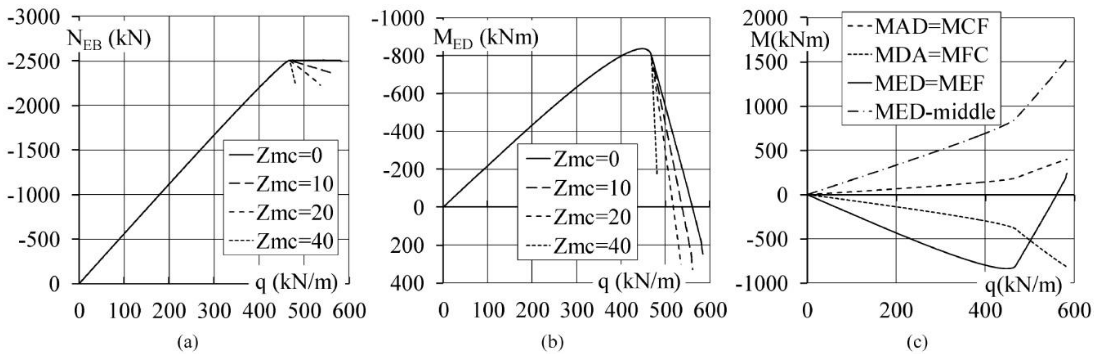

Fig. 12 Response and internal force redistribution in frame of Example 2

3.3 Example 3: Examination structural ductility to transverse loading

The frame of Fig. 13 was designed based on Eurocodes 2 and 8 to resist both static and seismic loads. The frame is subjected to a gravity dead load G, and a gravity live load Q followed by a transverse pseudo-static seismic force E. When subjected to gravity alone the frame fails for a total load $q_{collapse}$=85kN/m. Figure 14 presents the relation of gravity load q with the mid-span deflection u_z. The levels of service load (G+Q), failure load (1.35G+1.5Q), and collapse load $q_{collapse}$ are also presented. It is noted that the failure load corresponds to the formation of the first plastic hinge at the girder mid-span, while the collapse load corresponds to the formation of three plastic hinges on the girder. It becomes clear in this example that there exists a significant reserve load in excess of the code-defined failure. The extent of this reserve depends on the level of redundancy of the structure.

This example also demonstrates the influence of the intensity of the gravity load q, as a fraction of $q_{collapse}$, on the transverse strength and ductility of this frame.

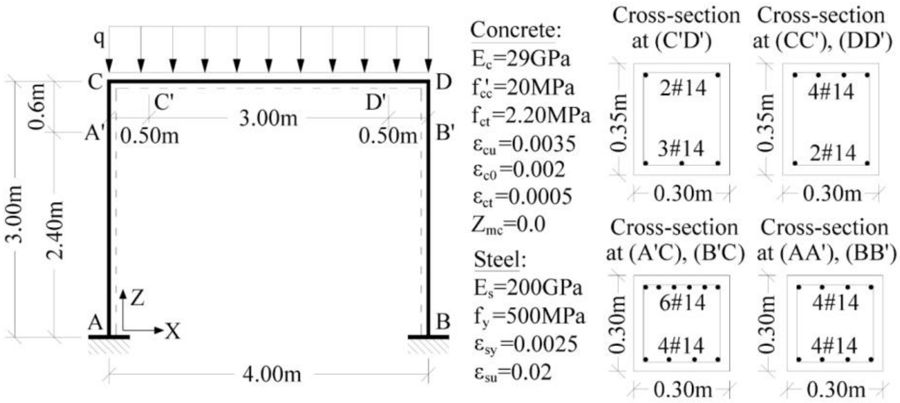

Fig. 13 Frame subjected to axial compression followed by transverse displacement

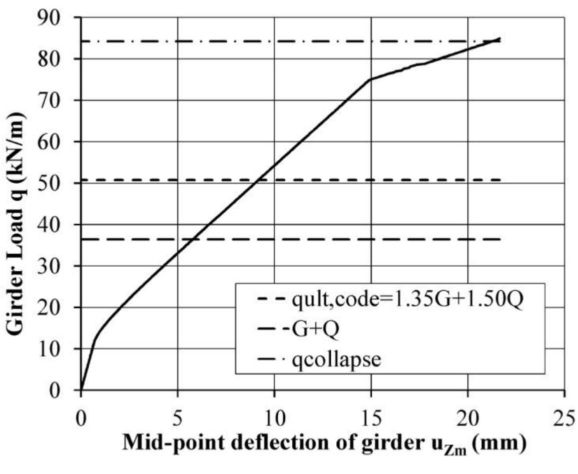

Fig. 14 Deflection of the girder mid-point as a function of the frame gravity load q

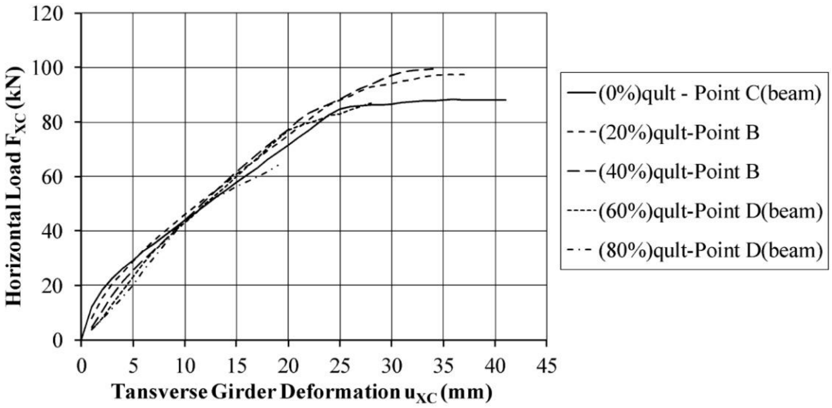

Fig. 15 Influence of gravity load on transverse strength and ductility

The frame is loaded at different fractions of the failure gravity load $q_{collapse}$, followed by a transverse load to the point where the first failure occurs. The outcome of this analysis is presented in Fig. 15. The transverse resistance of the frame depends on the stiffness of the columns and the level of fixity of the girder to the top of the columns. As the gravity load increases, the axial load and the negative end moment of each column increase in magnitude. Based on the interaction diagrams, small applications of gravity forces, load the columns below the balance point, and have beneficial effects on the capacity of the frame to carry transverse loads. When gravity forces increase sufficiently, the columns are loaded above the balance point, and gradually lose their capacity to carry transverse loading. In all cases, however, the effects of gravity loading result in reduced transverse ductility (smaller deformations to failure).

3.4 Example 4: Softening response to gravity loading

The frame of Fig. 16 represents the bottom story of a multi-story structure. The transfered loads from the upper stories to nodes C and D are P_z=802kN and P_x=400kN as shown in Fig. 16. It is noted that the loads P_z at nodes C and D correspond to approximately 80% of the balanced failure axial compression of the column cross-sections.

The girder is then loaded by a distributed load q_u to failure. The response of the frame to the distributed load q_u is presented in Fig. 17. It is noted that the load path of the columns, as presented in Fig. 17b, is caused by the application of q_u, while the more trivial axial compression path caused by loads P_z and leading to an initial axial compression of the columns is not emphasized.

The frame fails at a load q_u=650kN/m. At that point, the girder develops plastic hinges at its ends and midpoint, and cannot carry additional load. The end plastic hinges develop first at the load q_u=503kN/m. Additional loading results in softening of these plastic hinges, as indicated in Fig. 17a. The softening occurs due to the loading path of the column, which intersects the M-N interaction diagram above the balance point (Fig. 17b). Thus, increase of axial compression results in loss of bending strength of the column, and leads to plastic hinge softening. Nevertheless, the frame load carrying capacity increases passed the plastic hinge load due to redistribution. This example demonstrates the ability of the algorithm presented in this study to handle softening without encountering computational instabilities.

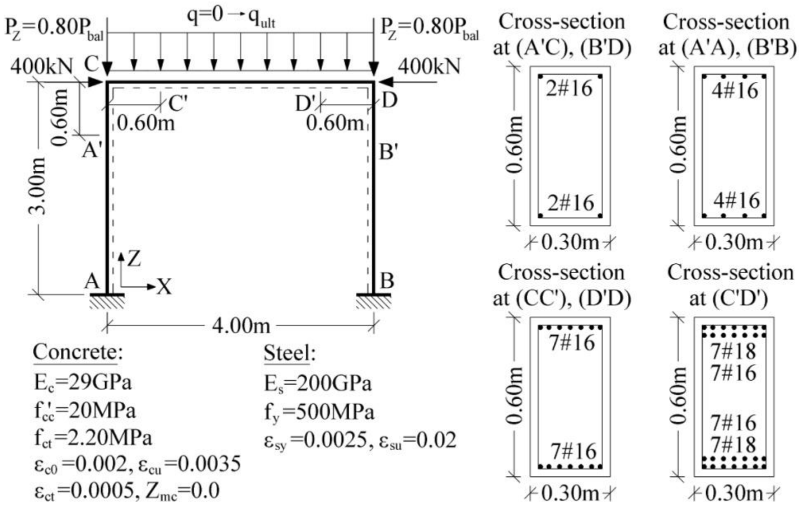

Fig. 16 Frame with significant softening behavior

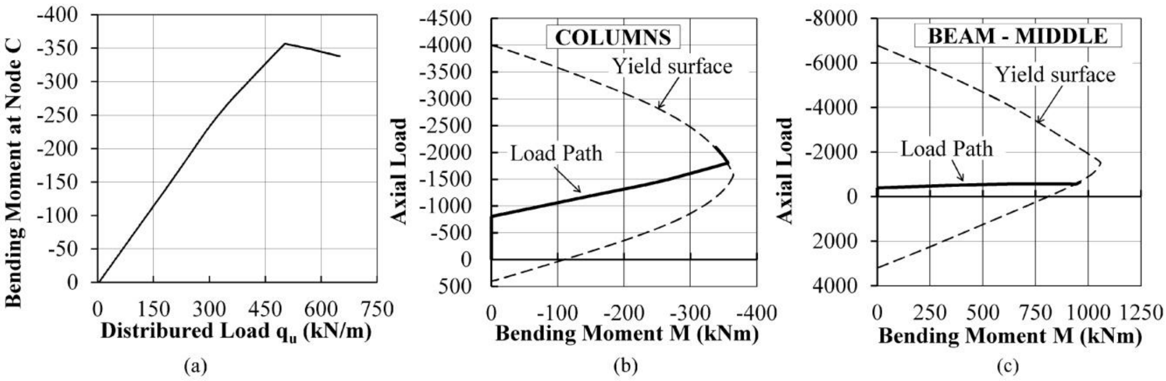

Fig. 17 Influence of the M-P interaction diagram in the development of forces of a concrete frame: (a) Development of bending moment at the column-beam joint, (b) Load path progression of bending moment at girder end, limited by the M-P interaction diagram and (c) Load path progression of bending moment at girder middle

4. Conclusions

A new approach is presented in this paper to model the nonlinear behavior of structures that are subjected to overloads. The nonlinear behavior is achieved using nonlinear stiffness matrices with degrading axial rigidity EA and bending stiffness EI, based on the instantaneous element strength as decided by the N-M interaction diagrams. As opposed to the elastic approach, element subdivision of a physical structural element is required to capture the variable levels of non-linearity along the length of a member based on the local stress intensity. Simple examples are used to a) validate the accuracy of the method; b) demonstrate the importance of using nonlinear analysis, where significant deviations from the elastic solutions, including moment reversals may occur; c) demonstrate factors that influence transverse load capacity and ductility of frames; and d) demonstrate the ability of this algorithm to address problems with softening without problems of numerical instabilities. Through these examples, it is demonstrated that a nonlinear analysis can capture structural response that cannot be predicted by the common elastic analysis – ultimate strength design approach, which is typically followed by practicing structural engineers. Noteworthy conclusions drawn from the examples presented here include:

1. Strength reserve may exist beyond that predicted by the code. The level of this reserve depends on the level of redundancy of the structure.
2. Depending on the selected strength and stiffness of individual members, the internal force redistribution may become extensive enough to cause bending moment reversals. Such redistribution, if not properly addressed may have detrimental effects on the structure.
3. Load paths with increasing axial compression above the balance point of the interaction diagram, or decreasing axial compression below the balance point result in reduction of the bending moment capacity and eventual softening behavior, which must be addressed in the design.
4. The capacity and ductility of frames when subjected to transverse loads, depends significantly on their gravity loads. Whereas the transverse load capacity initially increases with gravity loads before it eventually decreases, the ductility of the structure continuously decreases with increased gravity loads.

It is noted that the significant strength reserves that redundant structures have, is typically sufficient to account for potential softening and loss of ductility. However, statically determinate structures, or structures of low redundancy may be vulnerable to unpredicted local or global failures due to unaccounted nonlinear behavior.

References

Bouchaboub, M., Samai M.L. (2013), “Nonlinear analysis of slender high-strength R/C columns under combined biaxial bending and axial compression”, *Eng. Struct.*, **48**, 37-42.

Comite Euro-International du Beton (CEB) (1993), “CEB-FIP model code 1990”, CEB Bulletin d’ Information 213-214, Thomas Telford Service Ltd., London, England.

Cranston, W.B. (1965), *Tests on Reinforced Concrete Frames 1: Pinned Portal Fra*mes, Technical Report TRA/392, Cement and Concrete Association, London, England.

El-Metwally, S.E., El-Shahha, A.M., and Chen, W.F. (1990), “3-D nonlinear analysis of r/c slender columns”, *Comput. Struct.*, **37**(5), 863-872.

Eurocode 2 (2004), *Design of concrete structures - Part 1-1: General rules and rules for buildings*, European Committee for Standardization, Brussels, Belgium.

Eurocode 8 (2004), *Design of structures for earthquake resistance - Part 1: General rules, seismic actions and rules for buildings*, European Committee for Standardization, Brussels, Belgium.

Fantilli, A.P., Mihashi, H. and Vallini, P. (2007), “Crack profile in RC, R/FRCC and R/HPFRCC members in tension”, *Mater. Struct.*, **40**, 1099–1114.

Gregori, J.N., Sosa, P.M., Prada, M.A.F. and Filippou, F.C. (2007), “A 3D numerical model for reinforced and prestressed concrete elements subjected to combined axial, bending, shear and torsion loading”, *Eng. Struct.*, **29**(12), 3404-3419.

Hognestad, E., Hanson, N.W. and McHenry, D. (1955), “Concrete stress distribution in ultimate strength design”, *J. Ame. Concrete Inst.*, Part 1, **27**(4), 455-479.

Hu, H.T., Lin, F.M. and Jan, Y.Y. (2004), “Nonlinear finite element analysis of reinforced concrete beams strengthened by fiber-reinforced plastics”, *Compos. Struct.*, **63**(3-4), 271-281.

Karabinis, A.I. and Kiousis, P.D. (2001), “Plasticity model for reinforced concrete elements subjected to overloads”, *ASCE J. Struct. Eng.*, **27**(11), 1251-1256.

Kent, D.C. and Park, R. (1971), “Flexural members with confined concrete”, *J. Struct. Div., Proceeding of the American Society of Civil Engineers*, **97**(ST7), 1969-1990.
King, W.S., White, D.W. and Chen, W.F. (1992), “Second-order inelastic analysis methods for steel-frame design”, *ASCE J. Struct. Eng.*, **18**(2), 408-428.
Koshikawa, T. (2013), “Modelling the postpeak stress-displacement relationship of concrete in uniaxial compression”, *VIII International Conference on Fracture Mechanics of Concrete and Concrete Structures*, Van Mier, J.G.M, Ruiz, G. Andrade, C., Yu, R.C., and Zhang, X.X. (Eds), Toledo, Spain.
Liew, J.Y.R. (1992), “Advanced analysis for frame design”, Ph.D. Dissertation, West Lafayette: Purdue University.
Nanakorn, P. (2004), “A two-dimensional beam-column finite element with embedded rotational discontinuities”, *Comput. Struct.*, **82**, 753-762.
Powell, G.H. and Chen, P.F.S. (1986), “3D Beam-Column element with generalized plastic hinges”, *J. Eng. Mech.*, **112**(7), 627-641.
Sharma, R.M. (1990), “Ductility analysis of confined colu
mns”, *J. Struct. Eng.*, **116**(11), 3148-3161.
Song, H.W., You, D.W., Byun, K.J. and Maekawa, K. (2002), “Finite element failure analysis of reinforced concrete T-girder bridges”, *Eng. Struct.*, **24**(2), 151-162.
Spacone, E., Ciampi V. and Filippou, F.C. (1996), “Mixed Formulation of Nonlinear Beam Finite Element”, *Comput. Struct.*, **58**(1), 71-83.
Stevens, N.J., Uzumeri, S.M., Collins, M.P. and Will, G.T. (1991), “Constitutive model for reinforced concrete finite element analysis”, *ACI Struct. J.*, **88**(1), 49-59.
White, D.W. (1993), “Plastic hinge methods for advanced analysis of steel frames”, *Journal of Construct. Steel Res.*, **24**(2), 121-152.
Yüksel, E. and Karadoğan, F. (2009), “Simplified calculation approach of load deformation relationships of a beam-column element”, *G. U. J. Sci.*, **22**(4), 341-350.

CC